Stellar neutron capture cross section of the unstable *s*-process branching point ^{151}Sm

K. Wisshak, F. Voss, and F. Käppeler*

Forschungszentrum Karlsruhe, Institut für Kernphysik, Postfach 3640, D-76021 Karlsruhe, Germany

M. Krtička

Faculty of Mathematics and Physics, Charles University, CZ-180 00 Prague, Czech Republic

S. Raman†

Oak Ridge National Laboratory, Oak Ridge, Tennessee, 37831-6354, USA

A. Mengoni

CERN, CH-1211 Geneva 23, Switzerland, and IAEA, Nuclear Data Section, P.O. Box 100, A-1400 Vienna, Austria

R. Gallino

Dipartimento di Fisica Generale, Università di Torino, Sezione INFN di Torino,
Via P. Giuria 1, I-10125 Torino, Italy and Centre for Stellar and Planetary Astrophysics,
School of Mathematical Sciences, Monash University 3800, Victoria, Australia

The neutron capture cross sections of the radioactive isotope ^{151}Sm and of natural samarium have been measured in the energy range from 3 keV to 225 keV at the Karlsruhe 3.7 MV Van de Graaff accelerator. Neutrons were produced via the ^{7}Li$(p, n)^{7}$Be reaction by bombarding metallic Li targets with a pulsed proton beam and capture events were registered with the Karlsruhe 4π Barium Fluoride Detector. The cross sections were determined relative to the gold standard using a 206 mg sample of samarium oxide with 90% enrichment in ^{151}Sm. Over most of the measured energy range uncertainties of $\sim$2–3% could be achieved for the ^{151}Sm/^{197}Au ratio. Maxwellian averaged neutron capture cross sections of ^{151}Sm were calculated for thermal energies between $kT = 8$ keV and 100 keV with due consideration of the stellar enhancement factor and were found to be systematically larger than all previous theoretical predictions used in the analysis of the *s*-process branching at ^{151}Sm. In the context of the branching analysis, an experimental determination of the stellar enhancement factor due to captures in thermally excited states is proposed, and the tentative determination of the *p*-process residual of ^{152}Gd and a few other cases is discussed.

I. INTRODUCTION

In the course of the experimental program with the Karlsruhe 4π BaF$_2$ detector, which is focused on measurements of keV neutron capture cross sections of relevance for the main component of *s*-process nucleosynthesis, the present work on ^{151}Sm represents the first measurement on a highly radioactive sample. The mass region of the rare earth isotopes is particularly interesting because the relative abundances are well defined. This allows us to study the many branchings in this part of the *s*-process reaction path free from the systematic uncertainties in the elemental abundances that often hamper such analyses in other mass regions. Quantitative analyses of the important branchings provide a unique test for the underlying stellar models of the He burning conditions of thermally pulsing low mass AGB stars [1,2]. The neutron capture cross section of ^{151}Sm is a crucial part of the nuclear physics input for a thorough branching analysis and is, therefore, required with good accuracy.

The *s*-process reaction path in the vicinity of samarium is sketched in Fig. 1. This region is characterized by the four *s*-only isotopes ^{148,150}Sm and ^{152,154}Gd, which are shielded against possible *r*-process contributions by their stable Nd or Sm isobars. While ^{150}Sm is not affected by any branching, its abundance can be used for normalization of the total *s*-process reaction flow, whereas the branching to ^{152}Gd is strongly influenced by the branching at ^{151}Sm. The strength of the right arm of this branching to ^{152}Sm is particularly sensitive to the neutron capture rate $\lambda_n = n_n \times v_T \times \langle\sigma\rangle$, where n_n stands for the neutron density, v_T for the mean thermal velocity, and $\langle\sigma\rangle$ for the stellar (n, γ) cross section. The left arm is determined by the β^- decay rate of ^{151}Sm, which is significantly enhanced at *s*-process temperatures compared to the terrestrial value due to the decay of thermally populated excited nuclear states [3]. The minor branching at ^{152}Eu has only a marginal effect on the ^{152}Gd abundance, whereas there might be a considerable contribution from the *p* process as well.

The ^{151}Sm branching was first analyzed in 1984 based on activation measurements on some Sm, Eu, and Gd isotopes [4]. An improved data set was established in 1986 by a time of flight experiment on three samarium isotopes including the important *s*-only nuclei [5]. For the stable isotopes involved,

---

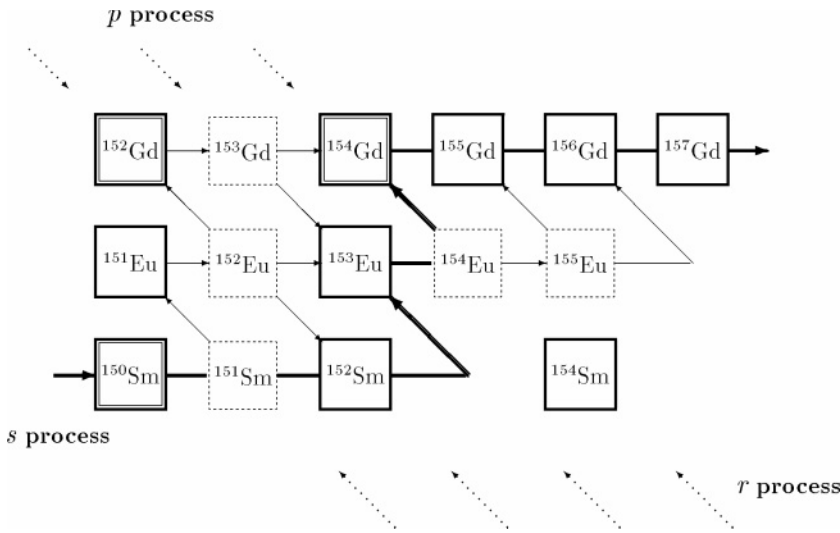*Electronic address: franz.kaeppeler@ik.fzk.de
†Deceased.

FIG. 1. The *s*-process network in the mass region of ^{151}Sm. Branchings of the reaction path occur at ^{151}Sm, ^{152,154,155}Eu, and ^{153}Gd. The branching effect at ^{152}Eu is completely dominated by the β-decay rate, which is strongly enhanced at stellar temperatures. Branching point nuclei and *s*-only isotopes are indicated by dashed and double boxes, respectively.

the data basis in this mass range was decisively extended by measurements on five Sm and six Gd isotopes with the Karlsruhe 4π BaF$_2$ detector [6,7] which could be used to derive an updated value for the *s*-process neutron density [8]. More recently, the branchings were discussed in the light of improved cross sections of the stable Eu isotopes [9].

The only cross section measurements on radioactive branching points in the mass region of interest here were measured for ^{147}Pm [10] and for ^{155}Eu [11] by means of the activation technique. Since the activation technique can not be applied for the determination of the ^{151}Sm cross section, all previous branching analyses had to resort to theoretical values for this important isotope. For a thermal energy of $kT = 30$ keV these calculated cross sections varied between 1542 mb and 2809 mb [12]. These discrepancies were too large for a meaningful branching analysis and triggered, therefore, the measurement reported here as well as at the CERN n_TOF facility [13].

The measurements in the neutron energy range from 3 keV to 225 keV and the corresponding data analysis are described in Secs. II and III, followed by a description of computer simulations with the GEANT code in Sec. IV. The discussion of the results and uncertainties is given in Secs. V and VI. The stellar cross sections and the astrophysical implications are addressed in Secs. VII and VIII. A full description of the present work, including data evaluation methods, calculation of correction factors, and the results from individual experimental runs can be found in Ref. [14].

II. EXPERIMENT

The (n, γ) cross section of ^{151}Sm has been measured relative to gold as a standard. Since the experimental method has been published in detail [6,15], only a general description is given here, complemented with the specific features of the present measurement.

Neutrons were produced via the ^{7}Li$(p, n)^{7}$Be reaction by bombarding metallic Li targets with the pulsed proton beam of the Karlsruhe 3.7 MV Van de Graaff accelerator. The neutron

energy was determined by time of flight (TOF), the samples being located at a flight path of 79 cm. The relevant parameters of the accelerator were a pulse width of <1 ns, a repetition rate of 250 kHz, and an average beam current of 2.0 μA. Runs with proton energies 30 keV and 100 keV above the threshold of the ^{7}Li$(p, n)^{7}$Be reaction provided continuous neutron spectra in the proper energy range for *s*-process studies, ranging from 3 keV to 100 keV, and from 3 keV to 225 keV, respectively. The lower proton energy was chosen to achieve a significantly better signal-to-background ratio at lower neutron energies.

Capture events were registered with the Karlsruhe 4π Barium Fluoride Detector [16] via the prompt capture γ-ray cascades. This detector consists of 42 hexagonal and pentagonal crystals forming a spherical shell of BaF$_2$ with 10 cm inner radius and 15 cm thickness. It is characterized by a resolution in γ-ray energy of 7% at 2.5 MeV, a time resolution of 500 ps, and a peak efficiency of 90% at 1 MeV. The 1.8 MeV γ-ray threshold in sum energy used in the present experiment corresponds to an efficiency for capture events of more than 95%.

The experiment was divided into three runs, two using the conventional data acquisition technique with the detector operated as a calorimeter, and one with an analog-to-digital converter (ADC) system coupled to the detector for analyzing the signals from all modules individually. In this way, the full spectroscopic information recorded by the detector can be recovered.

The preparation of the ^{151}Sm sample started already in 1990 during the experiment on the stable Sm isotopes [6]. Attempts to get hold of the metallic sample used in 1975 by Kirouac and Eiland for a measurement of the total cross section [17] were eventually successful in 1998 when ORNL agreed to reprocess the sample. The decay product ^{151}Eu was separated by liquid chromatography, the purified samarium oxide was heated to sufficiently high temperatures to ensure the proper stoichiometry and to eliminate possible water contaminations. It was pressed into a solid pellet 10 mm in diameter, which was enclosed in a Ti can prepared from 0.25 mm thick foils. The can consisted of a deep-drawn body 15 mm in diameter

TABLE I. Sample characteristics.

Sample	Diameter (mm)	Thickness		Weight (g)	Can[b] (g)	Neutron binding energy (MeV)
		(mm)	(10^{-3}at/barn)[a]			
Graphite	10.0	1.0	8.7427	0.1370	0.4349	
^{197}Au	10.0	0.4	2.1621	0.5554	0.4329	6.513
^{151}Sm[c]	10.0	0.6	0.8861	0.2064	0.4340	8.258
^{nat}Sm[c]	10.0	0.6	0.9675	0.2200	0.3989	5.6–8.1
Empty					0.4181	

[a]For Sm samples: sum of all Sm isotopes.
[b]Welded titanium can, lid and body deep-drawn from 0.25 mm thick foils.
[c]Chemical form Sm_2O_3.

with a 3 mm deep depression for the sample. The lid had a corresponding depression of 1 mm to match the 2 mm thick sample. The can was sealed by electron beam welding at the outer circumference of body and lid.

An identical sample was prepared from natural samarium oxide to verify the experimental procedures by checking whether the cross section of natural samarium could be properly reproduced.

Apart from the two samarium samples, a gold sample in an identical can was used for measuring the neutron flux, and an empty can served for determining the sample-independent background. The background due to scattered neutrons was measured by means of a corresponding graphite disk. The relevant sample parameters are compiled in Table I.

The change of isotopic composition with time in the ^{151}Sm sample was followed in detail, starting from a measurement at ORNL immediately after the Eu separation. When the sample was shipped to FZK 1.5 years later an updated isotopic composition was provided by ORNL corresponding to the ingrowth of ^{151}Eu. Since most of the measurements at FZK were carried out between October 2002 and January 2003, the composition at the end of November 2002 (fourth column in Table II) was adopted in data analysis. At this time the sample contained 156.8 mg of ^{151}Sm, 2% less than immediately after production. The ^{151}Eu impurity required a significant correction since this isotope has the largest keV capture cross section of all stable isotopes in this mass range.

The measured spectra of all samples were normalized to equal neutron flux by means of a ^{6}Li glass monitor located close to the neutron target. The transmission spectra measured with a second ^{6}Li glass detector 30 mm in diameter at a flight path of 260 cm could be used for a rough determination of the total cross section, since the sample diameter of 10 mm is just sufficient to shade the neutron monitor completely.

The samples were moved cyclically into the measuring position by a computer controlled sample changer. The spacing of the samples was 4 cm to ensure that the ^{151}Sm sample, which was mounted in the central position (Table I), was always completely within the inner radius of the spherical BaF_2 shell. In this way, the background due to the ^{151}Sm decay was similar in the spectra of all samples.

The measuring time per sample was about 10 min, a complete cycle lasting ~0.8 h. From each event, a 64 bit word was recorded containing the sum energy and TOF information together with 42 bits identifying the contributing detector modules. The relevant parameters of the three experimental runs are given in Ref. [14]. The data of run III were recorded with the ADC system. Run I had to be interrupted for nearly a year due to extensive repairs of the accelerator and to the fact that the ^{151}Sm sample was used in a parallel experiment at CERN [18,19]. This delay could be compensated in the other two runs when the averaged pulsed proton beam current was reaching a record of 2.8 μA at 250 kHz repetition rate, the largest value ever achieved at the Karlsruhe Van de Graaff.

TABLE II. Isotopic composition of the ^{151}Sm sample (in %) at different times.

Isotope	Eu separation (Oct. 28, 1999)	Shipping (May 21, 2001)	Measurement (Nov. 28, 2002)
^{144}Sm	0.05	0.051	0.052
^{147}Sm	1.37	1.384	1.398
^{148}Sm	0.22	0.222	0.224
^{149}Sm	0.40	0.404	0.408
^{150}Sm	3.93	3.972	4.013
^{151}Sm	90.05	89.945	89.842
^{152}Sm	3.32	3.355	3.389
^{154}Sm	0.66	0.667	0.674
mass Sm_2O_3 (mg)	206.4	204.24	202.16
mass Eu_2O_3 (mg)	0.0	2.16	4.24

TABLE III. Total cross sections (in barns) measured with the ^{6}Li glass detector at 260 cm flight path.

Neutron energy (keV)	^{151}Sm present	^{nat}Sm		^{12}C			^{197}Au	
		present	Ref. [6]	present	previous	JEFF[a]	present	previous
10–15	26.7	19.8	21.1	4.74	4.57	4.69	19.0	15.7
15–20	37.9	22.7	17.4	4.58	4.54	4.67	18.5	14.8
20–30	25.2	17.9	17.6	4.78	4.59	4.65	15.1	14.0
30–40	16.9	13.6	15.2	4.31	4.39	4.61	12.7	13.2
40–60	15.8	13.3	14.1	4.61	4.54	4.57	12.3	12.3
60–80	11.7	10.6	12.4	4.33	4.44	4.49	10.5	11.4
80–100	12.5	12.1	11.6	4.37	4.22	4.45	11.4	10.8
100–150	11.4	11.6	10.9	4.14	4.18	4.36	10.4	10.6
150–200	10.2	11.1	9.7	3.95	3.95	4.22	9.1	9.0
10–100	17.2	13.9	14.3	4.49	4.44	4.54	12.8	12.4
Typical uncertainty (%)	2.1	2.2	5.3	1.2	1.1		1.5	3.3

[a]Reference [20].

In total, the analyzed data were collected in a measuring time of ~45 d.

III. DATA ANALYSIS

A. Total cross sections

The total cross sections of the investigated isotopes were determined in the neutron energy range from 10 to 200 keV via the TOF spectra measured with the ^{6}Li glass detector at a flight path of 260 cm. The total cross sections and the related uncertainties were obtained as described in Ref. [6], and are listed in Table III. For easier comparison of the individual results the averaged total cross sections in the neutron energy interval from 10 to 100 keV are indicated as well. The results deduced for the carbon sample agree within ±1.2% with the data from the JEFF-3.1 evaluated data library [20] given in the seventh column of the table.

Since the first determination of the total cross sections of carbon and gold during the experiment on the stable samarium isotopes [6] these cross sections were redetermined in nine further experiments on isotopes of Ba, Gd, Sn, Nd, Dy, Yb, Cd, Lu, and Hf. A survey of this large amount of data showed that rather consistent results were obtained using samples of different diameter (15 and 22 mm) and different thickness (1.4 to 4.9 mm). The present results, which were obtained with samples 10 mm in diameter, are in good agreement with the averaged values of these ten experiments (columns labeled "previous" in Table III), except for the lowest energy bins, which suffer from unfavorable signal/background ratios.

The cross section of natural samarium was calculated from the values in Ref. [6] with the assumption that the total cross sections of ^{144}Sm and ^{154}Sm, which had not been measured, can be approximated by those of the neighboring even isotopes ^{148,152}Sm. This crude evaluation is in fair agreement with the present experiment (see Table III) and with the data given in Ref. [21].

The quoted uncertainties of the present measurements were obtained under the assumption that they are inversely proportional to the fraction of neutrons interacting in the sample, $A = 1 - T$, where T is the transmission. For the carbon sample this fraction is $A = 4.0\%$, the related uncertainty of 1.2% being estimated from the comparison with the JEF data.

B. Capture cross sections

The analysis was carried out in the same way as described previously [6,15]. All events were sorted into two-dimensional spectra containing 128 sum energy versus 2048 TOF channels according to different multiplicities (evaluation 1). In evaluation 2, this procedure was repeated by rejecting events, where only neighboring detector modules contributed to the sum energy signal. With this option, background from the natural radioactivity of the BaF$_2$ crystals and from scattered neutrons can be reduced. For all samples, the resulting spectra were normalized to equal neutron flux using the count rate of the ^{6}Li glass monitor close to the neutron target. The corresponding corrections are below 0.5% for all runs.

In the next step of data analysis, sample-independent backgrounds were removed by subtracting the spectra measured with the empty can. A remaining constant background was determined at very long flight times, where no time-correlated events are expected.

At this point, the spectra contain only events correlated with the sample. The next correction to be made is for isotopic impurities. Since samples of the impurity isotopes were not included in the present experiment this correction could not be achieved by a simple subtraction of the corresponding spectra. Based on the isotopic composition (Table II) and on the stellar cross sections at $kT = 30$ keV from Ref. [12] one can estimate that 95.2% of the events around 30 keV neutron energy should be due to capture in ^{151}Sm. Another 1.8% of events are contributed by capture in the impurity isotopes of
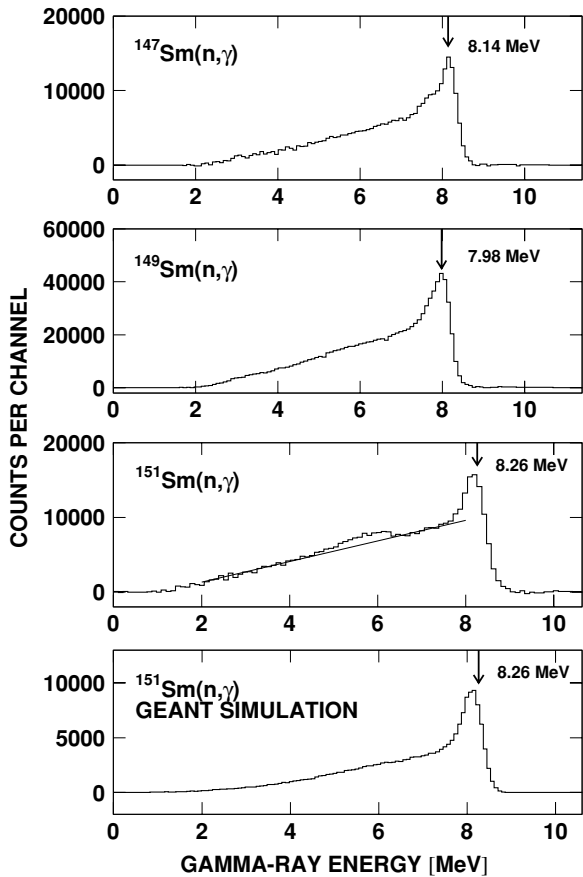
FIG. 2. The comparison of the measured sum-energy spectrum of ^{151}Sm with those of the stable odd Sm isotopes [6] and with a GEANT simulation for ^{151}Sm (bottom) confirms the linear behavior in the energy range between 2 MeV and 7 MeV assumed for evaluating the isotopic correction. All spectra contain only events with multiplicities >2.
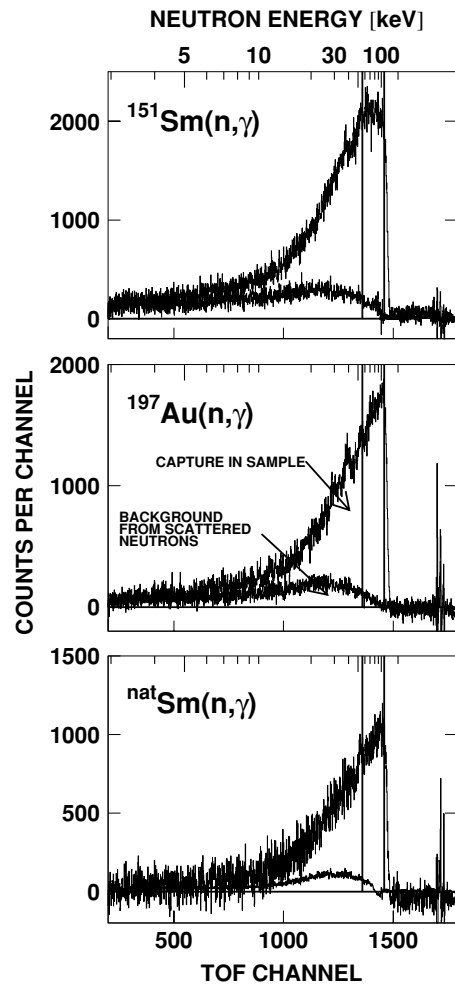

FIG. 3. TOF spectra measured in run III (100 keV maximum neutron energy) with the background due to sample scattered neutrons. The region used for absolute normalization of the cross section is indicated by two vertical lines.

samarium and 3.0% by capture in ^{151}Eu. The 1.8% correction for the Sm isotopes is due to contributions of 1.0% and 0.8% from the even and odd isotopes, respectively.

In Fig. 2 the sum-energy spectrum of capture events in ^{151}Sm is compared to the respective spectra of the two odd isotopes, ^{147}Sm and ^{149}Sm (from Fig. 5 of Ref. [6]) as well as with a simulation using the GEANT package (to be described in Sec. IV). From this comparison it is plausible to assume that the spectrum of capture events in ^{151}Sm is well represented by a straight line in the energy interval between 2 MeV and 7 MeV.

The correction for isotopic impurities was, therefore, performed in the following way. The energy dependence of the ^{151}Sm cross section was evaluated by using only events with sum energies above ∼6.5 MeV. This excluded automatically the contributions of the even samarium isotopes and of ^{151}Eu. For the absolute normalization of the cross section, where the sum-energy spectrum had to be integrated in the normalization interval from the adopted threshold at 1.8 MeV to energies above the binding energy (see below) a linear dependence of the spectral shape was assumed, eliminating events above the line shown in Fig. 2.

The remaining background due to capture of sample scattered neutrons was corrected by means of the data measured with the scattering sample. The binding energy of ^{151}Sm of 8.26 MeV is low enough, that this correction could be normalized via the pronounced sum-energy peak at 9.1 MeV from neutron captures in ^{135}Ba and ^{137}Ba. The corresponding signal-to-background ratios are illustrated in Fig. 3, where the contributions from scattered neutrons are indicated as well.

After this correction the spectra contain only the net capture events of the investigated isotopes. The cross section as a function of neutron energy was determined from the TOF spectra of Fig. 3, which are obtained by integrating the two-dimensional spectra in a region around the full energy peak. For the ^{151}Sm sample this range was restricted to events above 6.5 MeV. For absolute normalization, the two-dimensional data were projected onto the sum-energy axis using the TOF region with optimum signal/background ratio between the vertical lines indicated in Fig. 3. The resulting pulse height spectra are plotted in Fig. 4 for events with multiplicities >2. The spectrum of the natural Sm sample is dominated by the
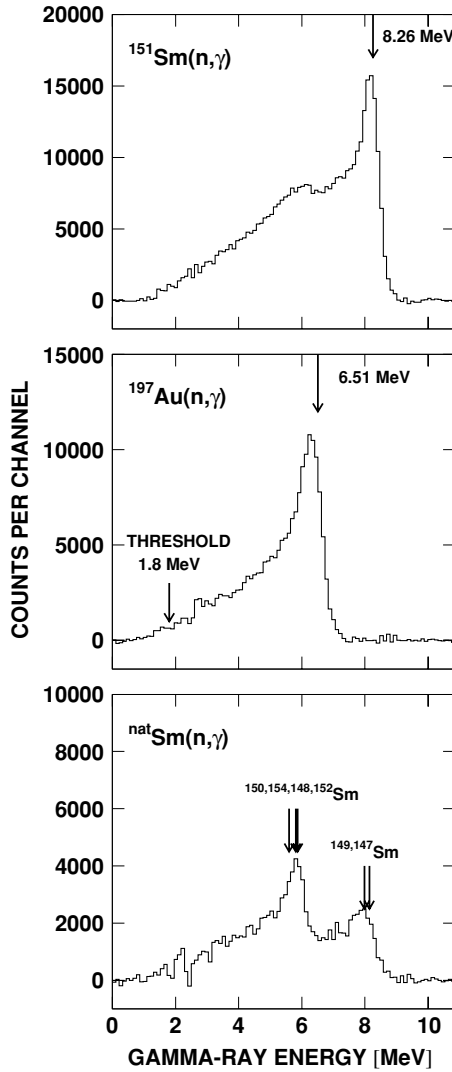
FIG. 4. Sum energy spectra measured in run III containing events with multiplicities >2 only. These spectra were obtained by projection of the two–dimensional spectra in the TOF region below the maximum neutron energy as indicated by vertical lines in Fig. 4.
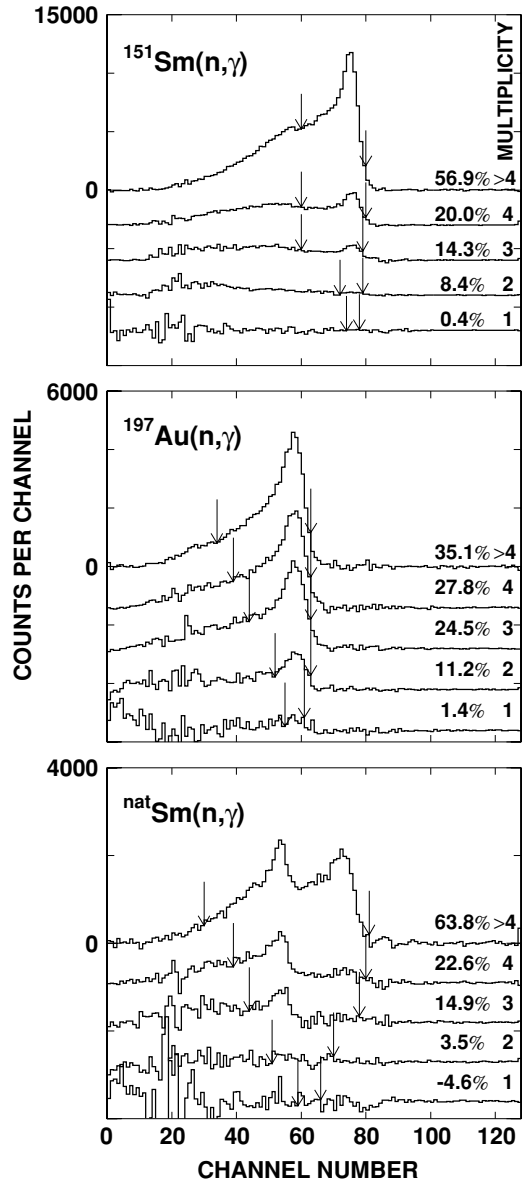

FIG. 5. Sum energy spectra of all isotopes as a function of multiplicity (run III). The regions used for determining the cross section shape (see TOF spectra of Fig. 3) are indicated by arrows. In the spectrum of the ^{151}Sm sample events below 6.5 MeV are excluded to avoid backgrounds from the main isotopic impurities. For better clarity the spectra for different multiplicities are shifted with respect to each other.

even isotopes. The contribution of the odd isotopes is slightly larger than in the ^{151}Sm sample due to the different isotopic composition.

The sum energy spectra of all isotopes are shown in Fig. 5 for different multiplicities. These multiplicities correspond to the number of detector modules contributing per event, which are slightly larger than the true multiplicities because of cross talking. The arrows in Fig. 5 indicate the range of sum energy channels that were integrated to obtain the TOF spectra of Fig. 3 for determining the cross section shapes.

The cross section ratio of isotope X relative to the gold standard is given by

$$\frac{\sigma_i(X)}{\sigma_i(Au)} = \frac{Z_i(X)}{Z_i(Au)} \frac{\Sigma Z(Au)}{\Sigma Z(X)} \frac{\Sigma E(X)}{\Sigma E(Au)} \frac{m(Au)}{m(X)} F_1 F_2. \quad (1)$$

In this expression, Z_i is the count rate of channel i in the TOF spectrum and ΣZ is the TOF rate integrated over the interval used for normalization (vertical lines in Fig. 5). The total count

rate in the sum-energy spectra for all multiplicities in this TOF interval, ΣE, is obtained by integration of the corrected spectra from the 1.8 MeV threshold up to and including the full energy peak at the respective separation energy.

The small number of events at low γ-ray energies and for multiplicities 1 and/or 2 contributes significantly to the statistical uncertainty. From the previous Sm measurements [6] it was known that the spectrum with multiplicity 1 contributes only a very small fraction to ΣE for the odd isotopes. This was also confirmed for ^{151}Sm, where the GEANT simulations described in Sec. IV yielded a contribution of 0.6%, in

TABLE IV. Fraction of undetected capture events f (%), and the related correction factors F_1.

	Threshold in sum energy (MeV)			
	1.5	1.7	1.8	2.0
From measured capture cascades				
$f(\text{Au})$	5.14	5.90	6.29	7.05
$f(^{151}\text{Sm})$	0.84	1.08	1.20	1.44
$f(^{\text{nat}}\text{Sm})$	2.22	2.86	3.18	3.82
$F_1(^{151}\text{Sm}/\text{Au})$	0.957	0.951	0.949	0.943
$F_1(^{\text{nat}}\text{Sm}/\text{Au})$	0.970	0.969	0.968	0.966
From GEANT simulations				
$f(\text{Au})$	4.19	5.19	5.68	6.68
$f(^{151}\text{Sm})$	0.55	0.75	0.86	1.06
$F_1(^{151}\text{Sm}/\text{Au})$	0.963	0.955	0.951	0.943

good agreement with the data of run III (Fig. 5). Similarly good agreement with Ref. [6] was found for the multiplicity distribution of the gold sample. The situation in the two other runs was less consistent though.

The correction of ΣE for isotopic impurities assumed that the sum-energy spectrum of ^{151}Sm can be approximated by a straight line in the energy range between 2 MeV and 7 MeV as illustrated in Fig. 2. Corrections of 3.9%, 4.1%, and 3.7% were obtained for runs I to III, respectively. According to the above estimates the average correction of 3.9% is mostly due to the 3% contribution of ^{151}Eu, while the parts of the even and odd samarium isotopes were found to be 0.9% and 0.8%. The resulting total correction of 4.7% was used in the analysis of all runs.

The quantity m in Eq. (1) denotes the sample thickness in atoms/b. The factor $F_1 = [100 - f(\text{Au})]/[100 - f(X)]$ is used to correct for the fraction of capture events f below the experimental threshold in sum energy, where X refers to the respective samarium sample (Table IV), and F_2 is the ratio of the multiple scattering and self-shielding corrections.

The fraction of unobserved capture events, f, and the correction factor F_1 were calculated as described in Ref. [22]. The input for this calculation are the individual neutron capture cascades and their relative contributions to the total capture cross section as well as the detector efficiency for monoenergetic γ-rays. As in Ref. [23] this information was derived directly from the experimental data recorded with the ADC system in run III. From these data, only events close to the sum energy peak (see Fig. 4) were selected, which contained the full capture γ-ray cascade. This ensemble was further reduced by restricting the analysis to the TOF region with optimum signal-to-background ratio (vertical lines in Fig. 3). The correction factors F_1 are quoted in Table IV.

The correction for neutron multiple scattering and self-shielding was calculated with the SESH code [24]. Apart from the pairing energies [25] most of the input parameters for the ^{151}Sm sample were taken from Ref. [26]. Missing values were adopted from the calculation for ^{149}Sm in Ref. [6], but slightly modified in order to reproduce the measured capture cross section. For the natural samarium sample the parameters from

the previous measurement were used for all isotopes. The final parameters are listed in Ref. [14] together with the resulting correction factors F_2. In general, these corrections are smaller than 2%.

IV. CASINO/GEANT SIMULATIONS

Additional information on the shape of the capture γ-ray spectra and on the multiplicity distribution was obtained by a theoretical description of the neutron capture cascades based on the available information on the respective level schemes. These cascades were used as input for a complete simulation of the experiment with the GEANT [27] code, a technique that has been demonstrated to reproduce the measured sum energy spectra and multiplicity distributions quantitatively [28,29].

Sets of γ-ray cascades including the probability for emission of conversion electrons were calculated for neutron captures on ^{151}Sm and on ^{197}Au using the CASINO version [30] of the Monte Carlo code DICEBOX [31], which is particularly suited for keV neutron energies. Each of the GEANT simulations was carried out with a set of 2×10^5 neutron capture cascades. Within the individual cascades each step is marked to distinguish γ-ray and converted transitions.

In the simulations the GEANT database was updated with the most recent neutron and gamma cross sections. The complex geometry of the 4π BaF$_2$ array was modeled in detail including reflectors, photomultipliers, and all structural materials. The efficiency for γ-rays originating from the sample in the center of the detector was calculated including the effect of converted transitions. The deposited energy in the various detector modules was followed down to the experimental threshold of $\approx$50 keV. Since conversion electrons are easily absorbed and do not contribute to the scintillation signal in the barium fluoride crystals this effect is important for the correct description of sum energy spectra. The energy resolution of the individual crystals was taken into account by using the values measured with calibrated sources.

The simulated spectra of the individual crystals and the sum energy spectra were stored as a function of multiplicity (as defined in Sec. III). Events were found with multiplicities between 1 and 15, but with strongly decreasing probability for $\geqslant 6$, in good agreement with the measured multiplicity distribution [14].

The simulations provide an independent check of the correction for the fraction of capture events, which escaped detection. This correction contributes significantly to the overall systematic uncertainty of the final cross section. The respective spectrum fractions f below sum energy thresholds of 1.5 MeV and 2 MeV were deduced from the simulated spectra for ^{151}Sm and ^{197}Au, and are listed in the lower part of Table IV together with the corresponding correction factors F_1 for the cross section ratio relative to the gold standard. At the actual experimental sum energy thresholds of 1.7 MeV and 1.8 MeV the simulated results for F_1 agree with the values obtained from the experimentally measured cascades within 0.3% on average. This agreement between the independently determined corrections confirms the uncertainties assigned to this correction.

TABLE V. Final neutron capture cross section ratios of ^{151}Sm and ^{nat}Sm relative to ^{197}Au with statistical, systematic, and total uncertainties.

Energy bin[a] (keV)	$\frac{\sigma(^{151}\text{Sm})}{\sigma(^{197}\text{Au})}$	Uncertainty (%)			$\frac{\sigma(^{nat}\text{Sm})}{\sigma(^{197}\text{Au})}$	Uncertainty (%)		
		stat	sys	tot		stat	sys	tot
3–5	5.1766	17.0	1.9	17.0	0.8869	56.0	0.6	56.0
5–7.5	4.5172	7.5	1.9	7.7	0.8985	16.0	0.6	16.0
7.5–10	4.4857	5.6	1.9	5.9	0.8234	14.0	0.6	14.0
10–12.5	5.3337	4.0	1.9	4.4	0.9985	10.0	0.6	10.0
12.5–15	5.6682	3.5	1.9	4.0	0.9908	8.1	0.6	8.1
15–20	5.5837	2.0	1.9	2.8	0.9469	4.5	0.6	4.5
20–25	6.1048	1.7	1.9	2.5	1.1289	3.4	0.6	3.5
25–30	5.6615	1.5	1.9	2.4	1.0112	3.0	0.6	3.1
30–40	5.6217	1.2	1.9	2.2	0.9429	2.5	0.6	2.6
40–50	5.6438	1.2	1.9	2.2	1.0150	2.4	0.6	2.5
50–60	5.6083	1.2	1.9	2.2	1.0572	2.3	0.6	2.4
60–80	5.1157	1.1	1.9	2.2	0.9998	2.1	0.6	2.2
80–100	4.7008	1.1	1.9	2.2	1.0333	2.1	0.6	2.2
100–120	4.3067	1.1	1.9	2.2	0.9961	2.1	0.6	2.2
120–150	3.9689	2.1	1.9	2.8	0.9967	4.0	0.6	4.0
150–175	3.7748	2.3	1.9	3.0	0.9955	4.3	0.6	4.3
175–200	3.3679	2.5	1.9	3.1	0.9543	4.6	0.6	4.6
200–225	3.1516	4.3	1.9	4.7	0.9553	8.0	0.6	8.0

[a]Energy bins as used for calculating the Maxwellian averaged cross sections.

V. DIFFERENTIAL NEUTRON CAPTURE CROSS SECTIONS

The measured neutron capture cross section ratios and the respective statistical uncertainties of the investigated Sm samples and of ^{197}Au are listed in Ref. [14] for all runs and for the two evaluation methods discussed in Sec. III. The data are free of systematic differences with respect to the various runs and evaluations and well consistent within the quoted statistical uncertainties. Even for natural samarium, where the statistical uncertainties are systematically larger due to the five times smaller cross section, all deviations are well below 1σ.

As in previous studies with the 4π BaF$_2$ detector [6,15,32], the final cross section ratios were adopted from evaluation 2. The respective mean values are compiled in Table V together with the statistical, systematic, and total uncertainties. The energy bins are sufficiently fine to avoid systematic effects in calculating the Maxwellian averaged cross section (Sec. VII). In the energy bins from 15 to 200 keV statistical uncertainties below 2.0% and 4% could be obtained for the ^{151}Sm and for the natural samarium sample, respectively.

The measured ratios were converted into absolute cross sections using the gold data of Macklin [33] normalized by a factor of 0.989 to the absolute value of Ratynski and Käppeler [34] (Table VI). The uncertainties of the resulting values can be obtained by adding the 1.5% uncertainty of the reference cross section to the uncertainties of the respective cross section ratios. The energy dependence of the present results are compared in Fig. 6 with the values reported by the n_TOF collaboration [18,19]. Both data sets are in perfect agreement throughout the entire energy range, the present results being about two times more accurate.

VI. DISCUSSION OF UNCERTAINTIES

The determination of statistical and systematic uncertainties are discussed with respect to the particular features of the present experiment and follows the procedures described in detail elsewhere [6,15]. The various contributions to the overall uncertainties are compiled in Table VII.

TABLE VI. Neutron capture cross sections of ^{151}Sm and ^{nat}Sm (in mb).

Energy bin (keV)	$\sigma(^{197}\text{Au})$[a]	$\sigma(^{151}\text{Sm})$	$\sigma(^{nat}\text{Sm})$
3–5	2267	11734	2010
5–7.5	1727	7800	1552
7.5–10	1216	5454	1001
10–12.5	1067	5690	1065
12.5–15	878	4977	870
15–20	739	4125	700
20–25	600	3663	677
25–30	571	3231	577
30–40	500	2813	472
40–50	433	2446	440
50–60	390	2185	412
60–80	349	1787	349
80–100	298	1402	308
100–120	290	1250	289
120–150	274	1088	273
150–175	264	995	263
175–200	253	851	241
200–225	249	783	237

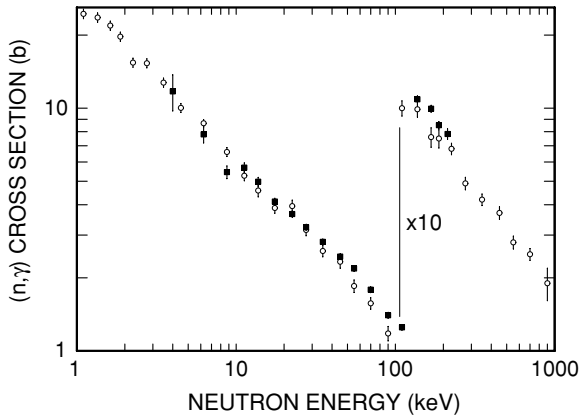[a]Based on the ^{197}Au data discussed in text.

FIG. 6. The measured neutron capture cross sections of ^{151}Sm (full squares) compared to the data from the n_TOF collaboration (open circles) [19].

The binding energy for the samarium isotopes is sufficiently low that the scattering background could be normalized in the sum energy region around 9 MeV and reliably subtracted. The resulting data from individual runs or related to the different acquisition modes and evaluation methods were free of systematic differences. The only exception found was the result for ^{151}Sm obtained in evaluation 1 of run II (Sec. V). Accordingly, systematic uncertainties in background subtraction were negligible as in the measurements on samarium [6], gadolinium [7], and dysprosium [23].

In contrast to previous experiments the count rate of the individual detector modules differed significantly due to the radioactivity of the ^{151}Sm sample. Though the Q-value for β^- decay is only 76.8 keV the corresponding background extends up to $\sim$200 keV. Above the electronic threshold of 50 keV the individual detector modules showed an average count rate of 12600 s^{-1}. Since the ^{151}Sm sample was shifted by only 4 cm from the central position when the gold sample was measured, the respective spectra exhibited almost identical backgrounds. This justified the assumption that the related systematic uncertainty was negligible. The systematic uncertainties due to the flight path measurement and the neutron flux normalization are also fairly small (Table VII).

TABLE VII. Systematic uncertainties (%).

Flight path	0.1
Neutron flux normalization	0.2
Sample mass: Elemental impurities	0.2
Isotopic composition (^{151}Sm only)	0.2
Isotopic correction (^{151}Sm only)	1.6
Multiple scattering and self–shielding: F_2	
$\quad$ ^{151}Sm/^{nat}Sm	0.3/0.4
Undetected events: F_1	
$\quad$ ^{151}Sm/^{nat}Sm	0.8/0.4
Total systematic uncertainties	
$\sigma(^{151}$Sm)/σ(Au)	1.9
$\sigma(^{nat}$Sm)/σ(Au)	0.6

The correction for the change in sample mass due to the decay of ^{151}Sm is slightly affected by the uncertainty of the half-life. The ^{151}Sm mass at the time of the measurement was determined using the value of $t_{1/2} = 93 \pm 8$ y of Reynolds [35], whereas the latest compilation recommends a half-life of 90 ± 8 y [36]. However, this difference translates only into a systematic uncertainty of 0.2% for the ^{151}Sm mass. The same uncertainty was assumed for the mass of the natural samarium sample, in this case to account for possible impurities [37].

The isotopic composition of highly enriched samples is commonly specified with absolute uncertainties of 0.2%. Though this seems to be rather conservative this value was adopted in the present ^{151}Sm analysis.

As shown in Fig. 2 events above the straight line were eliminated for each run separately, yielding an average isotopic correction of 3.9%. The spread of the individual results (Sec. III) was used to estimate a systematic uncertainty of 0.2%. However, this correction considered only events with sum energies between 4.8 MeV and 6.6 MeV. The low energy tail in the capture γ-ray spectra, which was missed due to lack of statistics, was estimated to 20% and 30% of the events for the odd and even isotopes, respectively. According to their different share in the correction, the respective contributions to the systematic uncertainty are 0.8% and 0.4%. Finally a fourth component of 0.2% was assumed for the contribution of the odd samarium isotopes. Altogether a systematic uncertainty of 1.6% was obtained for the isotopic correction of the ^{151}Sm data.

The uncertainty for the correction of multiple scattering and self-shielding was adopted from the output file of the SESH code. The calculation of the correction factors was carried out for a pure ^{151}Sm sample as well as for the actual sample including the isotopic impurities. Because the difference between both results was only $\approx$0.3%, the corresponding uncertainty is negligible.

The discussion of the systematic uncertainties due to undetected events [7] showed that uncertainties of the correction factor F_1 were 0.3% for the even and 0.8% for the odd isotopes. These corrections were based on two independent sets of calculated capture cascades, and were found to agree with the respective uncertainties quoted in previous measurements with the 4π BaF$_2$ detector [6,15,32]. It turned out that this uncertainty was mainly determined by the difference in binding energy between the investigated isotope and the gold standard, which is large for odd, but small for even isotopes. With this procedure, uncertainties of 0.8% and 0.4% were obtained for the correction factors F_1 of the ^{151}Sm sample and of the natural sample (effective binding energy 5.8 MeV), respectively. This uncertainty is confirmed by comparison with the independent determination of the correction factor F_1 in the GEANT simulations (Table IV).

VII. ASTROPHYSICAL IMPLICATIONS

A. Maxwellian averaged cross sections

Maxwellian averaged cross sections were calculated in the same way as described in Refs. [15,22]. The neutron energy range from 0–700 keV was divided into three intervals I_x

TABLE VIII. Maxwellian averaged (n, γ) cross section of ^{151}Sm.

kT (keV)	I_1 (0–3 keV) from Ref. [38][a] (mbarn)	I_2 (3–225 keV) this work (mbarn)	I_3 (225–700 keV) from Ref. [38][a] (mbarn)	$\langle \sigma v \rangle / v_T$ (mbarn)	stat	sys[b]	tot
8	1384 ± 134	5644 ± 203	0	7028	214	189	285
10	923 ± 92	5159 ± 150	0	6082	157	147	215
15	434 ± 43	4270 ± 85	0	4704	88	99	132
20	251 ± 25	3674 ± 58	0.1	3925	59	79	99
25	163 ± 16	3243 ± 44	0.8	3407	45	67	81
30	115 ± 12	2913 ± 35	3.1 ± 0.1	3031	36	59	69
40	65.5 ± 7	2429 ± 26	15.0 ± 0.4	2510	26	48	55
50	42.3 ± 4	2079 ± 21	36.6 ± 1.0	2158	21	41	46
52	39.1 ± 4	2020 ± 20	41.7 ± 1.2	2101	20	40	45
60	29.5 ± 3	1807 ± 18	83.8 ± 2.5	1920	18	36	40
70	21.8 ± 2	1586 ± 16	92.3 ± 2.9	1700	16	32	36
80	16.7 ± 2	1402 ± 14	119 ± 4	1538	15	29	33
90	13.2 ± 1	1248 ± 13	143 ± 5	1405	14	27	30
100	10.8 ± 1	1117 ± 11	164 ± 6	1291	12	25	28

[a]Normalized to present data.

[b]The 1.5% uncertainty of the gold cross section is not included, since it cancels out in most applications of relevance for nuclear astrophysics.

according to the origin of the adopted cross sections (see Table VIII). The dominant part I_2 between 3 keV and 225 keV is provided by the present experiment (Table VI). These data were obtained with sufficient resolution in neutron energy to exclude systematic uncertainties that may result in the calculation of the Maxwellian average if the energy grid is too coarse.

The contribution I_1 was determined by normalizing the cross sections of Kopecky *et al.* [38] to the present data in the interval between 3 keV and 50 keV. Since the shape of both data sets were found in reasonable agreement, an uncertainty of 10% was assumed for the contribution I_1.

At typical *s*-process temperatures the energy interval from 225 keV to 700 keV contributes very little to the Maxwellian average. For this part, the data of Kopecky *et al.* [38] were normalized to the present results between 100 and 225 keV, in order to account for a slightly different energy dependence of the evaluated data. The corresponding uncertainties were assumed to increase from 2% at 225 keV to 10% at 700 keV.

The systematic uncertainties of the Maxwellian averaged cross sections in Table VIII are determined by the uncertainties of the measured cross section ratios in the interval I_2 (Table V) as well as by the respective I_1 and I_3 contributions. The 1.5% uncertainty of the gold standard was not included since it cancels out in most applications of relevance for *s*-process studies. In general, the systematic uncertainties dominate over the statistical uncertainties, except at low thermal energies.

The present results at $kT = 30$ keV are eventually compared in Table IX with the result obtained by the n_TOF collaboration and with previous calculations quoted in the compilations of Bao *et al.* [12] and of Beer, Voss, and Winters [39]. The present result is in excellent agreement with the n_TOF value [18]

but significantly more accurate. It is surprising to see that the Maxwellian averaged (n, γ) cross section of ^{151}Sm was systematically underestimated in all theoretical calculations.

Before the experimental cross sections can be used in a stellar model code they must be corrected by the so-called stellar enhancement factor (SEF), which accounts for the fact that low-lying excited states can be thermally populated at typical *s*-process temperatures. These correction factors

$$\sigma^* \equiv \text{SEF} \times \sigma^{\text{lab}} \qquad (2)$$

are usually obtained via the Hauser-Feshbach statistical model theory (HFSM). While this correction is negligible for the even-even isotopes involved in the *s*-proces branching at $A = 151$, several low-lying levels in ^{151}Sm give rise to a significant SEF correction of this cross section. In particular, the population probability of the first excited state at 4.8 keV reaches 30 % at thermal energies of $kT = 30$ keV. Accordingly, this correction must be carefully evaluated.

TABLE IX. Maxwellian averaged (n, γ) cross section of ^{151}Sm (in mb) at $kT = 30$ keV compared to previous data.

Experiments		Calculations		Evaluations	
3031 ± 82	this work[a]	1542	[49]	1932 ± 206	[39]
3100 ± 160	[18]	1820 ± 460	[8]	2710 ± 420	[12]
		1932	[5]		
		2809	[50]		
		1990	[51]		

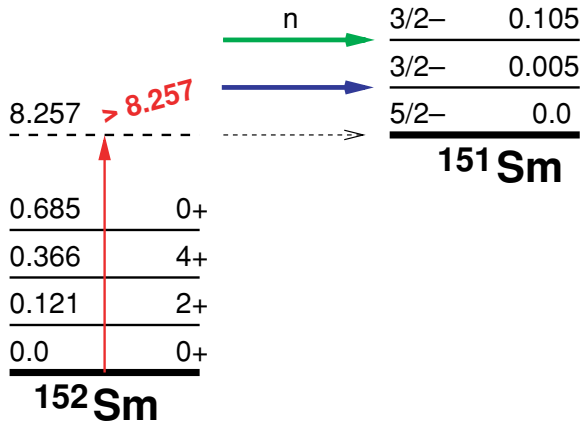[a]Here the 1.5% uncertainty of the gold cross section was included for a consistent comparison with Ref. [18].

FIG. 7. (Color online) Dissociation of ^{152}Sm into ^{151}Sm $+ n$.

The main ingredients for the corresponding HFSM calculations are the optical model parameters for the interaction of the neutron with the target, which yield the neutron transmission coefficients for the neutron-nucleus interaction as well as the density of nuclear states at excitation energies up to ≈ 1 MeV above the neutron separation threshold. Finally, the electric dipole resonance parameters are used to evaluate the γ-ray strength functions.

In this way, a SEF correction of 0.87 was obtained with the HFSM code NON-SMOKER at $kT = 30$ keV [40], while a value of 0.93 was reported from a similar calculation [41]. This discrepancy is most likely due to different parametrizations of the Hauser-Feshbach theory. This uncertainty can be avoided, since the neutron capture cross sections for the relevant excited states of ^{151}Sm are experimentally accessible by the inverse (γ, n) reaction on ^{152}Sm [41]. In this reaction only excited states in ^{151}Sm can be populated via the dominant $E1$ transitions and with s-wave neutrons in the continuum. As indicated in the sketch of Fig. 7, the $5/2^-$ ground state of ^{151}Sm can only be populated by emission of d-wave neutrons, whereas the $3/2^-$ first excited state at $E_x = 4.82$ keV is populated by emission of s-wave neutrons. The next possible excitation goes to the fifth excited state at $E_x = 104.8$ keV, also a $J^\pi = 3/2^-$ state.

The (γ, n) cross section is calculated with the HFSM theory using the nuclear level density parametrization fixed to reproduce the experimental level spacings at the neutron separation energies [42]. In the samarium case, this information is available for both isotopes involved [26]. The Moldauer optical model parameters [43] and the experimental parameters of the giant dipole resonance [44] have been used for the calculation of neutron transmission functions and of the γ-ray strength function, respectively. The cross section has been renormalized in order to reproduce the measured MACS of the ^{151}Sm$(n, \gamma)^{152}$Sm reaction. This normalization factor turned out to be 1.7 for the present HFSM calculations as well as for the NON-SMOKER result [40].

As shown in Fig. 8 up to ≈ 100 keV above threshold the only open channel is the dissociation leading to the first excited state in ^{151}Sm ($J^\pi = 3/2^-$). Correspondingly, this component provides the information for deriving the capture cross section for the first excited state of ^{151}Sm. With
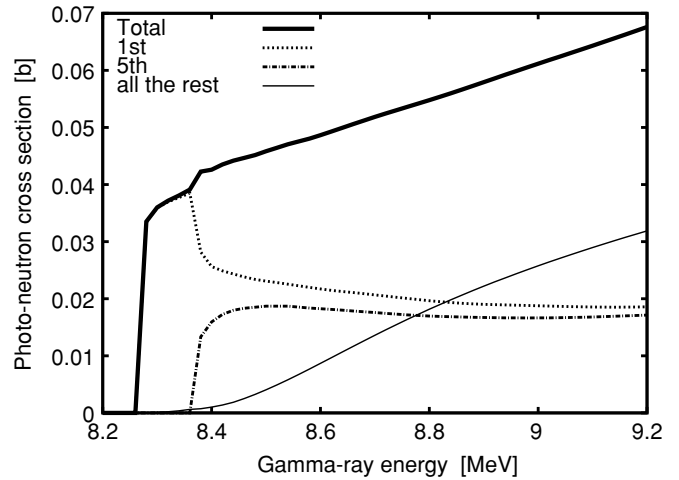

FIG. 8. HFSM calculation of the ^{152}Sm$(\gamma, n)^{151}$Sm cross section for dissociation into the different ^{151}Sm $+ n$ channels.

increasing excitation energy the second dissociation channel opens at $E_x = 104.8$ keV. Above this energy the cross section includes the effect of the neutron capture process in this state. Only at higher excitation energies, the effect of the ground state starts to contribute, but only at the level of a few percent.

The absolute value of the dissociation cross section is of the same order as that already measured for the ^{186}W$(\gamma, n)^{185}$W reaction [45].

B. Branching analysis and *s*-process yields

With this work and the parallel determination of the ^{151}Sm cross section in Refs. [18,19] all relevant stellar (n, γ) rates for a complete analysis of the *s*-process branching at ^{151}Sm have been accurately determined. Because of the very good agreement in the ^{151}Sm cross sections the branching analysis discussed in Ref. [19] is fully confirmed. This means that the present best set of nuclear input information can explain 77% and 91% of the *s*-only isotopes ^{152}Gd and ^{154}Gd, respectively (Fig. 1). While the underproduction of ^{154}Gd can be explained
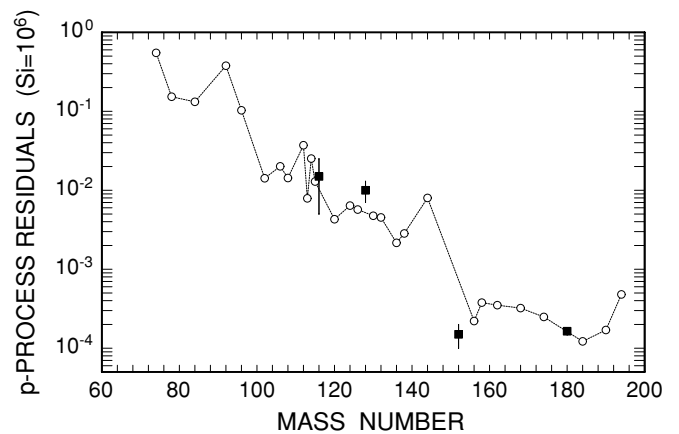

FIG. 9. Abundance distribution of *p*-only isotopes (open circles) and the *p*-process residuals listed in Table X (full squares).

TABLE X. *p*-process residuals, $N_p = N_\odot - N_s$ (normalized to Si $= 10^6$).

Isotope	$N_\odot^a$	N_s	$N_p = N_\odot - N_s$	Reference
^{116}Sn	5.55×10^{-1}	5.4×10^{-1}	$(1.5 \pm 1.0) \times 10^{-2}$	[46]
^{128}Xe	1.16×10^{-1}	1.06×10^{-1}	$(1.0 \pm 0.3) \times 10^{-2}$	[47]
^{152}Gd	6.6×10^{-4}	5.1×10^{-4}	$(1.5 \pm 1.0) \times 10^{-4}$	[19]
^{180}W	1.73×10^{-4}	8.6×10^{-6}	$(1.64 \pm 0.1) \times 10^{-4}$	[48]

^{a}Solar values are from Ref. [52].

by a modification of the MACS and/or the decay rate of ^{154}Eu, the missing ^{152}Gd abundance may correspond most likely to an additional *p* component (see below).

C. *p*-process residuals

If the difference between the observed abundance of ^{152}Gd and the calculated *s*-process yield is assumed to correspond to an additional *p*-process component, this should correlate with the overall distribution of the *p*-only isotopes. This comparison is illustrated in Fig. 9, where the abundances of the *p*-only

isotopes are plotted together with cases, where a similar *s*-process deficiency can be inferred.

Apart from ^{152}Gd, *p*-process residuals

$$N_p = N_\odot - N_s$$

have also been found for ^{116}Sn [46], ^{128}Xe [47], and ^{180}W [48] (Table X), which appear to fit rather well into the overall distribution. This can be taken as an additional confirmation that the stellar *s*-process model is capable of reproducing the observed *s*-process abundances with an accuracy of a few percent. However, any further conclusions seem to be premature at this point.

[1] R. Gallino, C. Arlandini, M. Busso, M. Lugaro, C. Travaglio, O. Straniero, A. Chieffi, and M. Limongi, Astrophys. J. **497**, 388 (1998).

[2] F. Käppeler, Prog. Part. Nucl. Phys. **43**, 419 (1999).

[3] K. Takahashi and K. Yokoi, At. Data Nucl. Data Tables **36**, 375 (1987).

[4] H. Beer, F. Käppeler, K. Yokoi, and K. Takahashi, Astrophys. J. **278**, 388 (1984).

[5] R. R. Winters, F. Käppeler, K. Wisshak, A. Mengoni, and G. Reffo, Astrophys. J. **300**, 41 (1986).

[6] K. Wisshak, K. Guber, F. Voss, F. Käppeler, and G. Reffo, Phys. Rev. C **48**, 1401 (1993).

[7] K. Wisshak, F. Voss, F. Käppeler, K. Guber, L. Kazakov, N. Kornilov, M. Uhl, and G. Reffo, Phys. Rev. C **52**, 2762 (1995).

[8] K. A. Toukan, K. Debus, F. Käppeler, and G. Reffo, Phys. Rev. C **51**, 1540 (1995).

[9] J. Best, H. Stoll, C. Arlandini, S. Jaag, F. Käppeler, K. Wisshak, A. Mengoni, G. Reffo, and T. Rauscher, Phys. Rev. C **64**, 015801 (2001).

[10] R. Reifarth, C. Arlandini, M. Heil, F. Käppeler, P. V. Sedyshev, M. Herman, T. Rauscher, R. Gallino, and C. Travaglio, Astrophys. J. **582**, 1251 (2003).

[11] S. Jaag and F. Käppeler, Phys. Rev. C **51**, 3465 (1995).

[12] Z. Y. Bao, H. Beer, F. Käppeler, F. Voss, K. Wisshak, and T. Rauscher, At. Data Nucl. Data Tables **76**, 70 (2000).

[13] U. Abbondanno *et al.*, Report CERN-SL-2002-053 ECT, CERN (2003).

[14] K. Wisshak, F. Voss, F. Käppeler, M. Krtička, and S. Raman, Report FZKA-6996, Forschungszentrum Karlsruhe (2004).

[15] K. Wisshak, F. Voss, F. Käppeler, and G. Reffo, Phys. Rev. C **45**, 2470 (1992).

[16] K. Wisshak, K. Guber, F. Käppeler, J. Krisch, H. Müller, G. Rupp, and F. Voss, Nucl. Instrum. Methods A **292**, 595 (1990).

[17] G. Kirouac and H. Eiland, Phys. Rev. C **11**, 895 (1975).

[18] U. Abbondanno *et al.*, Phys. Rev. Lett. **93**, 161103 (2004).

[19] S. Marrone *et al.*, Phys. Rev. C (this volume).

[20] JEFF-3.1 General Purpose Neutron File, May 2005, available at http://www.nea.fr/html/dbdata/JEFF/

[21] V. McLane, C. Dunford, and P. Rose, *Neutron Cross Sections*, Vol. 2 (Academic Press, New York, 1988).

[22] K. Wisshak, F. Voss, F. Käppeler, and G. Reffo, Phys. Rev. C **42**, 1731 (1990).

[23] F. Voss, K. Wisshak, C. Arlandini, F. Käppeler, L. Kazakov, and T. Rauscher, Phys. Rev. C **59**, 1154 (1999).

[24] F. Fröhner, Report GA-8380, Gulf General Atomic, (1968).

[25] A. Gilbert and A. Cameron, Can. J. Phys. **43**, 1446 (1965).

[26] J. Mughabghab, M. Divadeenam, and N. Holden, *Neutron Cross Sections*, Vol. 1, Part A (Academic Press, New York, 1981).

[27] J. Apostolakis, GEANT library, http://wwwinfo.cern.ch/asd/geant/(CERN).

[28] M. Heil, R. Reifarth, M. M. Fowler, R. C. Haight, F. Käppeler, R. S. Rundberg, E. H. Seabury, J. L. Ullmann, J. B. Wilhelmy, K. Wisshak, and F. Voss, Nucl. Instrum. Methods A **459**, 229 (2001).

[29] R. Reifarth, M. Heil, F. Käppeler, F. Voss, K. Wisshak, F. Bečvář, M. Krtička, R. Gallino, and Y. Nagai, Phys. Rev. C **66**, 064603 (2002).

[30] F. Becvár, in *Gamma-Ray Spectroscopy and Related Topics*, edited by S. Wender (American Institute of Physics, New York, 2000), p. 504.

[31] F. Bečvář, Nucl. Instrum. Methods A **417**, 434 (1998).

[32] F. Voss, K. Wisshak, K. Guber, F. Käppeler, and G. Reffo, Phys. Rev. C **50**, 2582 (1994).

[33] R. Macklin, private communication to Mughabghab, S.F. (1982), see also www.nndc.bnl.gov/nndc/ EXFOR 12720.002.

[34] W. Ratynski and F. Käppeler, Phys. Rev. C **37**, 595 (1988).

[35] S. Reynolds, J. Emery, and E. Wyatt, Nucl. Sci. Eng. **32**, 46 (1968).

[36] B. Singh, Nucl. Data Sheets **80**, 263 (1997).

[37] K. Wisshak, F. Voss, F. Käppeler, and L. Kazakov, Report FZKA-6961, Forschungszentrum Karlsruhe (2004).

[38] J. Kopecky, J.-Ch. Sublet, J. A. Simpson, R. A. Forrest, and D. Nierop, Report INDC(NDS)-362, International Atomic Energy Agency, Vienna, Austria (1997), data available at http://www-nds.iaea.or.at/ngatlas/main.htm.

[39] H. Beer, F. Voss, and R. Winters, Astrophys. J. Suppl. **80**, 403 (1992).

[40] T. Rauscher and F.-K. Thielemann, At. Data Nucl. Data Tables **79**, 47 (2001).

[41] A. Mengoni, in *Nuclear Data for Science and Technolgy*, edited by R. Haight and M. Chadwick (AIP, New York, 2005), p. 1209.

[42] A. Mengoni and Y. Nakajima, J. Nucl. Sci. Technol. **31**, 151 (1994).

[43] P. Moldauer, Nucl. Phys. **47**, 65 (1963).

[44] P. Carlos, H. Beil, R. Bergere, A. Lepretre, A. De Miniac, and A. Veyssiere, Nucl. Phys. **A225**, 171 (1974).

[45] K. Sonnabend, P. Mohr, K. Vogt, A. Zilges, A. Mengoni, T. Rauscher, H. Beer, F. Käppeler, and R. Gallino, Astrophys. J. **583**, 506 (2003).

[46] C. Theis, F. Käppeler, K. Wisshak, and F. Voss, Astrophys. J. **500**, 1039 (1998).

[47] R. Reifarth, F. Käppeler, F. Voss, K. Wisshak, R. Gallino, M. Pignatari, and O. Straniero, Astrophys. J. **614**, 363 (2004).

[48] F. Käppeler, C. Arlandini, M. Heil, F. Voss, K. Wisshak, R. Reifarth, O. Straniero, R. Gallino, S. Masera, and C. Travaglio, Phys. Rev. C **69**, 055802 (2004).

[49] T. Rauscher and F.-K. Thielemann, At. Data Nucl. Data Tables **75**, 1 (2000).

[50] M. Harris, Astrophys. Space Sci. **77**, 357 (1981).

[51] J. Holmes, S. Woosley, W. Fowler, and B. Zimmerman, At. Data Nucl. Data Tables **18**, 305 (1976).

[52] E. Anders and N. Grevesse, Geochim. Cosmochim. Acta **53**, 197 (1989).